Technical Note BN-461 July 1966

OSCILLATORY AND TRANSITORY EKMAN BOUNDARY LAYERS*

by

Alan J. Faller and Robert Kaylor

University of Maryland
College Park, Maryland

*The research reported here has been supported in part by the National Science Foundation under Grant GP-3443. The computational work was supported by National Aeronautics and Space Administration Grant NSG-398 to the Computer Science Center of the University of Maryland.

ABSTRACT

Time variations of the wind stress over the ocean cause the boundary-layer flow to be significantly different from that of the classical Ekman spiral. Simple analytical solutions for the cases of rotating and oscillating wind stresses are presented, and numerical solutions of the transitory boundary layers for more realistic wind variations are given. These solutions are basically extensions of Ekman's spiral solutions for the cases of a constant coefficient of viscosity and his "quadratic friction-relationship", and of Fredholm's solution for the case of a step function in wind stress. The results show that the large inertial oscillations discussed by Ekman for the case of constant viscosity are even more persistent when the "quadratic friction-relationship" is applied.

1. INTRODUCTION.

The now-classical paper of Ekman (1905) delineated the major features of the boundary-layer flow to be expected in the surface layers of the ocean due to wind stress, and the Ekman spiral that corresponds to a steady wind stress and a constant coefficient of viscosity is often cited. Among other specific but less well known results of Ekman's famous work are the transitory solution for a step function in the wind stress (attributed to Fredholm) and the steady spiral solution that corresponds to Ekman's "quadratic friciton-relationship". Our results extend the transitory solution presented by Ekman to other interesting variations of the wind stress, the intent being to examine and illustrate the degree to which the flow in the planetary boundary layer of the ocean may differ from that of a steady-state spiral as a result of temporal variations of the wind.

In addition to simple analytical solutions for rotating and oscillating wind stresses, we present numerical computations of the boundary-layer flow for more realistic variations of the wind for both a constant coefficient of viscosity

and for a coefficient of viscosity dependent upon the wind stress and the shear flow in the boundary layer. These studies were undertaken as an extension of our numerical studies of the instability of Ekman boundary layers (Faller and Kaylor, 1966) at the suggestion of Dr. P. Welander.

The equations of motion that describe the transitory Ekman boundary layer are:

$$\frac{\partial u'}{\partial t'} - 2\Omega v' = \frac{\partial}{\partial z'}\left(\nu \frac{\partial u'}{\partial z'}\right)$$

$$\frac{\partial v'}{\partial t'} + 2\Omega u' = \frac{\partial}{\partial z'}\left(\nu \frac{\partial v'}{\partial z'}\right) \qquad (1)$$

where the primes refer to dimensional variables. Horizontal gradients of the flow and the vertical velocity are taken to be zero, and there are no horizontal pressure gradients. The Cartesian coordinates are right-handed with z' vertically upward and the origin at the ocean surface, so that depth in the ocean is given by negative values of z'. To take into account the Coriolis force at some specific latitude ϕ it is only necessary to replace Ω by $\Omega \sin \phi$ throughout the analysis.

For the case of constant ν equations (1) are made non-dimensional by the following definitions:

$$u = u'/V_o' \quad , v = v'/V_o', \quad z = z'/D, \quad t = \Omega\, t'$$

where $D = (\nu/\Omega)^{\frac{1}{2}}$ is the characteristic depth of the Ekman boundary layer and

$$V_o' = (u'^2 + v'^2)^{\frac{1}{2}} \quad \text{at} \quad z = 0.$$

(Note that D as used here is smaller than the characteristic depth used by Ekman (here designated D_{Ek}) by the factor

$$D/D_{Ek} = 1/\pi.)$$

The non-dimensional equations are then:

$$\begin{aligned} \frac{\partial u}{\partial t} - 2v &= \frac{\partial^2 u}{\partial z^2} \\ \frac{\partial v}{\partial t} + 2u &= \frac{\partial^2 v}{\partial z^2} \end{aligned} \qquad (2)$$

For later reference, the steady-state Ekman solution to (2) that corresponds to a constant shear stress at the free surface and zero stress at $z = -\infty$ in our notation is:

$$\left.\begin{matrix} u \\ v \end{matrix}\right\} = e^{z} \left\{\begin{matrix} \cos \\ -\sin \end{matrix}\right\} \left(z + \frac{\pi}{4} + \theta\right) \qquad (3)$$

where θ is the angle between the stress and the positive x axis, and where we have used the boundary condition

$$dV/dz = \sqrt{2} \quad \text{at} \quad z = 0.$$

2. ROTATING AND OSCILLATING WIND STRESSES.

Since (2) are linear equations, the solution for an arbitrary variation of the wind stress may be composed from a sum (or integral) of linearly independent periodic solutions. For this reason, as well as for their intrinsic interest, we first discuss simple harmonic solutions with frequency k correspondent to harmonic variations of the wind stress with the same frequency.

An harmonically oscillating wind stress with fixed orientation (fixed θ) may be regarded as the sum of two vectors of constant magnitude rotating in opposite directions. Their rotation frequencies will be denoted by $\ell = \pm k$ where a positive value of ℓ indicates rotation in the cyclonic sense (in the direction of increasing θ) and a negative ℓ indicates anticyclonic rotation. Evidently, from the linearity of the equations, the solution for an oscillatory stress of amplitude 1.414 will be the sum of the solutions for the two oppositely rotating stresses of constant magnitude 0.707.

A single rotating stress of frequency ℓ may be written in component form as

$$\left.\begin{matrix}\tau_x \\ \tau_y\end{matrix}\right\} = 0.707 \left\{\begin{matrix}\cos \\ \sin\end{matrix}\right\} (\ell t + \theta) \tag{4}$$

where $\tau_x = du/dz|_o$ and $\tau_y = dv/dz|_o$. Assuming periodic solutions to (2) we write the resultant velocity components as

$$\left.\begin{matrix}u \\ v\end{matrix}\right\} = U(z) \left\{\begin{matrix}\cos \\ \sin\end{matrix}\right\} \left(\ell t + \Phi(z)\right) \tag{5}$$

where U and Φ are unknown functions of z. Substitution of (5) into (2) gives

$$\begin{aligned} -\left(\ell + 2\right)v &= \frac{\partial^2 u}{\partial z^2} \\ \left(\ell + 2\right)u &= \frac{\partial^2 v}{\partial z^2} \end{aligned} \tag{6}$$

which are identical in form to the steady-state portions of (2) and differ only in that the Coriolis terms are multiplied by $(1 + \ell/2)$. Thus the effect of a uniformly rotating stress, as opposed to a steady stress, is merely a modification of the effective rate of rotation of the coordinate system, and we anticipate that the solution to (6) will be an Ekman spiral

with modified amplitude and depth scales.

If we define a second non-dimensional depth by $z^* = z'/D^*$, where $D^* = (\nu/\Omega(1 + \frac{\ell}{2}))^{\frac{1}{2}}$, the solution of (6) is

$$\left.\begin{matrix} u \\ v \end{matrix}\right\} = \frac{D^*}{D} e^{z^*} \left\{\begin{matrix} +\sin \\ -\cos \end{matrix}\right\} (z^* + \ell t + \delta) \qquad (7)$$

where $\delta = \theta + \pi/4$, and where the ratio D^*/D arises from the new non-dimensionalization of the stress. The total solution for an oscillating stress is then the sum of the two solutions for $\ell = +k$ and $\ell = -k$ as follows:

$$\left.\begin{matrix} u \\ v \end{matrix}\right\} = (2K_1)^{-1} e^{K_1 z} \left\{\begin{matrix} +\sin \\ -\cos \end{matrix}\right\} (K_1 z + kt + \delta) + (2K_2)^{-1} e^{K_2 z} \left\{\begin{matrix} +\sin \\ -\cos \end{matrix}\right\} (K_2 z - kt + \delta) \qquad (8)$$

where $K_1 = +(1 + k/2)^{\frac{1}{2}}$, $K_2 = \pm(1 - k/2)^{\frac{1}{2}}$, and k is always positive. For K_2 the positive root is used when $k/2<1$, and the negative root applies when $k/2>1$.

Some examples of the solution (8) for $\delta = \pi/4$ are shown in Figures 1 and 2 for $k/2<1$ and $k/2>1$, respectively. For Figure 1 the two spirals correspond to $k = 1$ at the instant when both rotating vectors are oriented along the x axis. Since the velocity vectors at $z = 0$ have the amplitudes $A_1 = (2K_1)^{-1}$

and $A_2 = (2K_2)^{-1}$ it may readily be seen that the terminal point of the velocity at $z = 0$ executes an ellipse with the major axis 45 degrees to the left of the oscillating stress. The magnitude of the semi-major axis is $A_2 + A_1$ and that of the semi-minor axis $A_2 - A_1$. Figure 2 has been constructed for $k = 2\pi$ as an example of $k>2$. There it is shown that the spiral for $\ell<2$ is "left-handed". This may also be seen from (6) where for $\ell<-2$ the signs of the Coriolis terms are reversed and the spiral must be that correspondent to negative rotation of the coordinate system, the Southern Hemisphere case. Accordingly, for $k>2$ the major axis of the ellipse at $z = 0$ is along the x axis, the axis of the oscillating stress.

Figures 3 and 4 are examples of numerical solutions of (2) for $k = 1$ and $k = 2\pi$, respectively.* The computations started with zero flow, and as a result there were transitory components to the solutions, but it may be seen that the oscillations of the surface velocity approached the theoretical ellipses as discussed above. For $k = 1$ the theoretical semi-major axis is 1.114 and the semi-minor axis, 0.300. For $k = 2\pi$ the semi-axes are 0.588 and 0.096.

When $k = 2$ there is a singularity in the solution (8). This corresponds to resonance between the anticyclonically rotating

* The methods of numerical computation are discussed in the appendix and in Faller and Kaylor (1966).

component of the oscillating wind stress ($\ell = -2$) and inertial oscillations in the rotating system. Figure 5 is a numerical computation that shows the steady amplification of the surface velocity due to this resonance.

To more clearly see the resonant case, note that in an absolute reference frame the surface stress would be constant in magnitude and direction, and the governing equations would reduce to $\frac{\partial U}{\partial t} = \frac{\partial^2 U}{\partial z^2}$. The resultant flow would have the same constant direction at all depths, and an equilibrium solution could only be obtained for a finite depth of fluid.

3. A STEP FUNCTION IN THE WIND STRESS.

Ekman has presented an exact solution (found by Fredholm) for the case of an abrupt increase in wind stress from zero to a constant value, although the method of solution was not indicated. One method would be to integrate the solution (8) over k using as amplitudes for each oscillatory component those found from a Fourier integral representation of a step function in stress. A somewhat simpler procedure was outlined to us by Professor J. M. Burgers and is as follows:

The velocity components are expressed in the complex notation $w = u + iv$ and the set (2) is written

$$\frac{\partial w}{\partial t} + 2iw = \frac{\partial^2 w}{\partial z^2}. \tag{9}$$

If we assume a solution of the form $w = A\, e^{pt + \lambda z}$ it follows from (9) that $\lambda = (p + 2i)^{\frac{1}{2}}$. Then let $A = (\sqrt{2}\ \pi\ ip(p + 2i)^{\frac{1}{2}})^{-1}$ so that the shear at the free surface, dw/dz at $z = 0$, has the value 0 for $t>0$ and the value $\sqrt{2}$ for $t<0$. This follows since $\int e^{pt}/\ p\ dp = 2\pi i$ for $t>0$ and 0 for $t<0$. The integral for w is then

$$w = (\sqrt{2}\pi i)^{-1} \int p^{-1}\ (p + 2i)^{-\frac{1}{2}} \exp\ (pt + (p+ 2i)^{\frac{1}{2}})\ dp \tag{10}$$

If equation (10) is differentiated with respect to time we obtain

$$\frac{\partial w}{\partial t} = (2\pi i)^{-\frac{1}{2}} \int (p + 2i)^{-\frac{1}{2}} \exp\ (pt + (p + 2i)^{\frac{1}{2}} z)\ dp \tag{11}$$

which must be essentially the integral solved by Fredholm. In particular, at $z = 0$ equation (11) may readily be integrated to give

$$w(z = 0) = (2/\pi)^{\frac{1}{2}} \int_0^t \zeta^{-\frac{1}{2}} e^{-2i\zeta} d\zeta \tag{12}$$

where ζ is a dummy time variable. Equation (12) is the Fresnel integral (Jahnke and Emde, 1945) that describes the Cornu spiral (see Figure 6).

Ekman graphically presented Fredholm's solution by diagrams of velocity vs. time at various depths. As a check on our numerical methods (anticipating other applications) we obtained the numerical solution starting with (2), and we found precise agreement with Ekman's results at all depths. Figure 6 shows the solution at $z = 0$ with time expressed in pendulum hours for direct comparison with Ekman's diagram. The particular feature of note is the large inertial oscillation (period of 12 pendulum hours) which damps only inversely as the square root of time.

We have also computed the transitory response to a step function in wind for the variable coefficient of viscosity which Ekman called the "quadratic friction-relationship". In our notation the quadratic viscosity, in which "the frictional forces were proportional to the square of the rate of gliding", is given by

$$\nu = L^2((du'/dz')^2 + (dv'/dz')^2)^{\frac{1}{2}} \qquad (13)$$

where L is a mixing length that is independent of z'. Ekman's

steady-state solution to (1) using (13) is an equiangular spiral, but with the constant angle of 49.1 degrees between the velocity and the vertical shear compared to 45.0 degrees for the case of constant viscosity.* Since there was no exact correspondence between the characteristic depths of the two spirals, Ekman arbitrarily adopted $D' = 0.8\ Z'$ for comparison with the characteristic depth D_{Ek}, where $Z' = 1.16\ L^{\frac{1}{2}}\ (\tau/\rho w)^{\frac{1}{4}}\Omega^{-\frac{1}{2}}$ is the depth at which the velocity vanishes in the case of quadratic viscosity.

Our numerical results for a step function in stress and using the relation (13) are presented in Figure 7 which shows the time variations of the velocities at the depths $z' = 0$, $0.5\ D'$, and $1.0\ D'$, these for comparison with Ekman's figures at the comparable depths for the case of constant viscosity. The principal difference of note in the two transitory solutions is that for the quadratic viscosity the inertial oscillation damped much more slowly. At $z = 0$ it appears that the inertial oscillation decays as $t^{-\frac{1}{4}}$ (Figure 7) compared to the decay rate of $t^{-\frac{1}{2}}$ for constant viscosity (Figure 6).

4. VARIABLE WIND STRESS.

The original intent of this work was to integrate the boundary-layer flow over time for a variable wind stress similar

* A third equiangular spiral of interest (54.7 degrees) is that found by Rossby (1932) using (13) under the assumption of a linear decrease of L with distance from the free surface, rather than constant L.

to that which may occur over the ocean. To this end we have performed two separate integrations: 1) the case with constant viscosity and with the surface stress linearly proportional to the wind speed; 2) the case of quadratic viscosity with the stress proportional to the square of the wind and with the mixing length linearly proportional to the wind. The first case would correspond to a laminar laboratory situation, and the second more closely approximates turbulent oceanic conditions.

The variation of wind that was applied may be seen in Figures 8 and 9, which correspond to the two cases listed above, respectively. The time of each hodagraph is expressed in radians of rotation of the coordinate system, 1 unit corresponding to 3.82 hours. The sequence of wind vectors represents the following meteorological events at some point over the ocean: The wind started from $W = 0$, the center of a high pressure system. As the High moved eastward a low pressure center approached the point in question, and the wind increased steadily to $W = 15$ m s^{-1} with constant direction from the SE. At $t = 4.0$ a warm front passage gave an abrupt shift of the wind, and in the warm sector of the approaching Low the wind held constant at $W = 10$ m s^{-1} from SSW. At $t = 6.0$ a cold front passed and the wind shifted sharply to WNW at $W = 20$ m s^{-1}. Thereafter the wind decreased slowly with

nearly constant direction to $W = 0$ at $t = 10$. The cycle was then restarted for a short period, which accounts for the hodagraphs at times $t>10$. This wind variation incorporates a steadily increasing wind and abrupt shifts in the wind direction. It does not include all meteorologically interesting situations that may occur and was meant only as a typical sequence due to passage of large-scale pressure systems.

In Figure 8 depths are indicated on the hodagraphs in terms of the characteristic depth D, and the wind and velocity scales are arbitrary. Figure 9, the case of quadratic viscosity, is meant to correspond to the real ocean and we have expressed wind speeds in meters per second, flow speeds in centimeters per second, and depths in meters. In an attempt to realistically account for a decrease of mixing length as the free surface is approached from below, we have added a logarithmic boundary layer to the top of each spiral solution of Figure 9, in the manner of Rossby and Montgomery (1935). The circled point on each hodagraph indicates the point of attachment of the logarithmic layer to the spiral.

Details of the quadratic viscosity and logarithmic boundary layers are the following: Equations (1) were integrated using the relation (13). The spiral solutions were computed with the aid of the following two assumptions, applicable at 45 degrees

latitude: 1) The mixing length was taken proportional to the wind speed by the relation $L = W/5$ seconds; and 2) The wind stress was taken proportional to the square of the wind speed by the relation $(\tau/\rho_w)^{\frac{1}{2}} = u_w^* = 20 \times 10^{-2} W$, where u_w^* is the friction velocity for the water. The superposed logarithmic layer was computed from the equation

$$|\Delta \underset{\sim}{y}'| = u_w^*/k \left[\ln \left(\frac{-H + z'_{ow}}{z'_{ow}} \right) - \ln \left(\frac{-z' + z'_{ow}}{z'_{ow}} \right) \right] \qquad (14)$$

where $|\Delta \underset{\sim}{y}'|$ is the magnitude of the velocity to be added to the spiral solution in the direction of the wind. $H = L/k - z'_{0w}$ is the depth of the logarithmic layer, and $k = 0.4$ is von Karman's constant. The roughness length for the water was taken to be related to the wind by $z'_{ow} = 10^{-2} W$ seconds.

For the most part the above relations are based upon empirical formulas from various sources (Rossby and Montgomery, 1935; Sverdrup, 1942) and a complete justification would be too lengthy for this presentation. In the last analysis they are justified only in so far as they produce reasonable approximations to reality. The relations for z'_{ow} is based upon some recent (unpublished) observations by one of the authors (Faller) of the differential drift of floats and tracers near the surface of the

ocean, but this value should be regarded only as a preliminary estimate.

The most noteworthy aspect of Figures 8 and 9 is the rapid development of large inertial oscillations. In accord with the results of Section 3, these are considerably greater for the case of the quadratic viscosity, as may be seen particularly well near the time $t = 10$ when the wind dropped to zero. Since inertial oscillations decay so slowly due to viscosity, continued application of wind stress variations probably would lead to a large accumulation of inertial energy. In the real ocean, however, because of horizontal variations or the presence of side boundaries, inertial oscillations will normally produce oscillating pressure gradients that will result in both horizontal and vertical fluxes of inertial energy, neither of which are possible in the limited local model that we have used. As a result, we have not considered it to be profitable to extend the integrations over longer period of time.

With respect to the variation of wind that was chosen for this example, it should be noted that the wind rotated anticyclonically, correspondent toa location in the ocean to the south of the path of the low pressure center. It may be anticipated that if the wind rotated predominantly cyclonically, the resultant inertial oscillations would be somewhat smaller, and the amplitude

of the spiral flow would also be less, in accord with the results found in Section 2 for rotating stress vectors of constant magnitude.

A P P E N D I X

The methods of numerical integration.

A detailed discussion of finite-difference methods, stability criteria, and other pertinent material was presented in an earlier paper concerned with the stability of Ekman boundary-layer flow (Faller and Kaylor, 1966). These details will not be reconsidered here, and the interested reader should refer to the earlier work. However, the following changes were required:

1) The numerical solution was computed for a single vertical line of grid points, rather than for a two-dimensional field of points.

2) The applied pressure gradient, which was the source of the basic geostrophic flow in the earlier work, was eliminated.

3) The upper boundary condition of zero stress was replaced with a condition of constant stress or a specified variation of stress with time. There was no change in the lower boundary condition.

4) The numerical stability criterion $\nu\Delta t'/\Delta z'^2<0.25$ which arises from the viscous terms had to be replaced by the new criterion $L^2(dV'/dz')_{z=0}\Delta t'/\Delta z'^2<0.20$ for those cases with the quadratic viscosity. This criterion was determined empirically by trial and error.

REFERENCES

Ekman, V. W., 1905: On the influence of the Earth's rotation on ocean-currents. Arkiv foer Matematik, Astronomi, och Fysik, 2, No. 11, 1 - 52.

Faller, A.J. and R. E. Kaylor, 1966: A numerical study of the instability of the laminar Ekman boundary layer. J. Atmos. Sci., 23, (in press).

Jahnke, E. and F. Emde, 1945: Tables of Functions, 4th ed. Dover Publications, New York, 304 pp.

Rossby, C. -G., 1932: A generalization of the theory of the mixing length with application to atmospheric and oceanic turbulence. Meteor. Papers, 1, No. 4. Mass. Inst. Tech.

Rossby, C. -G., and R. B. Montgomery, 1935: The layer of frictional influence in wind and ocean currents. Papers in Physical Ocean. and Meteor., 3, No.3. Mass. Inst. of Tech. and Woods Hole Ocean.Inst.

Sverdrup, H.U., 1943: Oceanography for Meteorologists. Prentice-Hall, Inc. New York, 235 pp.

Figure 1. Theoretical solution for an oscillating wind stress with angular frequency k = 1 and amplitude 1.414. The solid spiral hodagraph corresponds to the cyclonically rotating component (ℓ = 1) with magnitude 0.707, and the dashed spiral corresponds to the anticyclonically rotating component (ℓ =-1) of the same magnitude. Depths are in terms of D for the steady Ekman spiral.

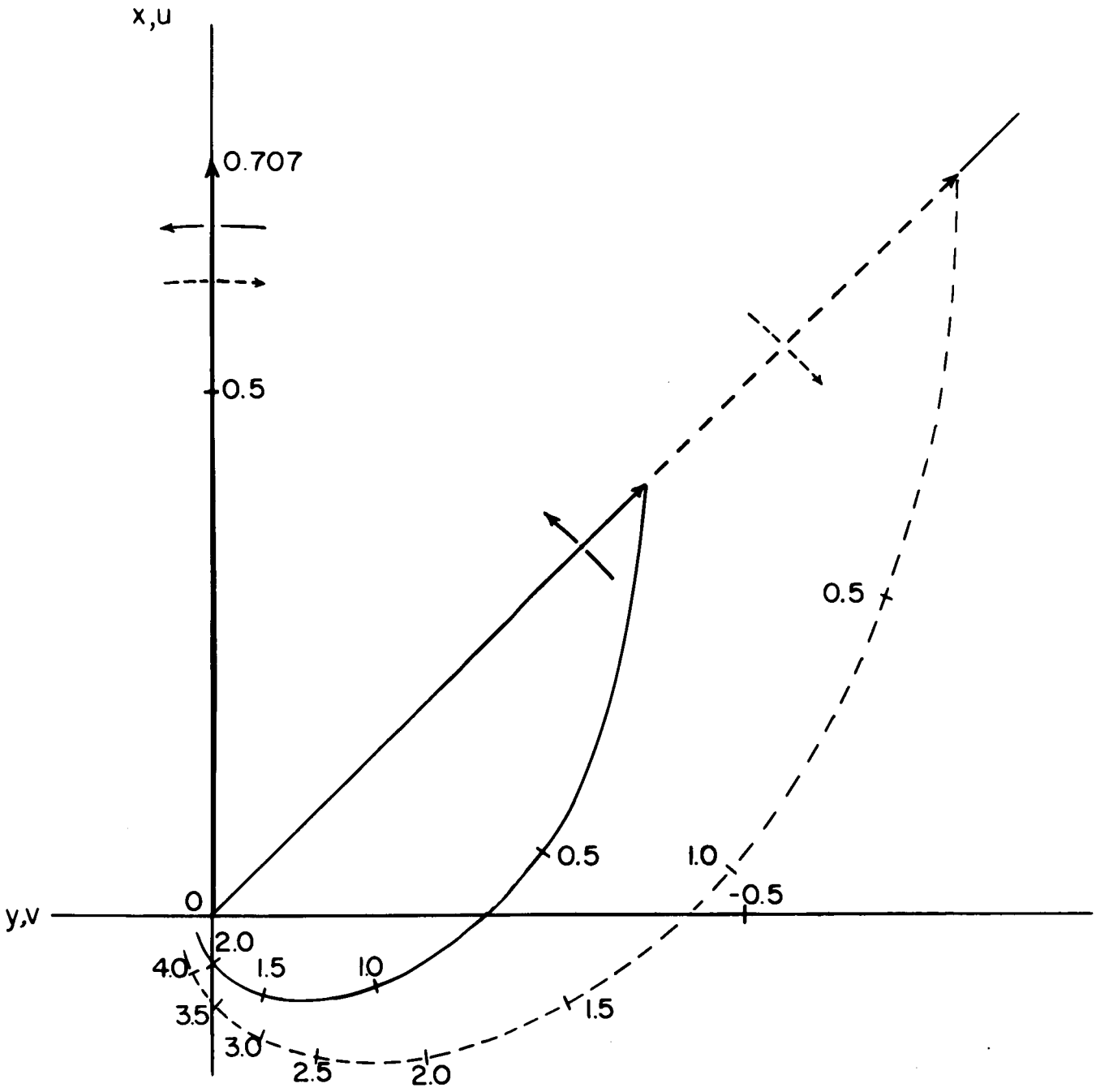
x,u
0.707
0.5
0.5
0.5
1.0
-0.5
y,v
0
2.0
4.0
1.5
1.0
3.5
3.0
2.5
2.0
1.5

Figure 2. Theoretical solution for an oscillating wind stress with angular frequency $k = 2$ and amplitude 1.414. The solid spiral corresponds to the cyclonically rotating stress ($\ell = 2$), and the dashed spiral corresponds to the anticyclonic component ($\ell = -2$), each of magnitude 0.707.

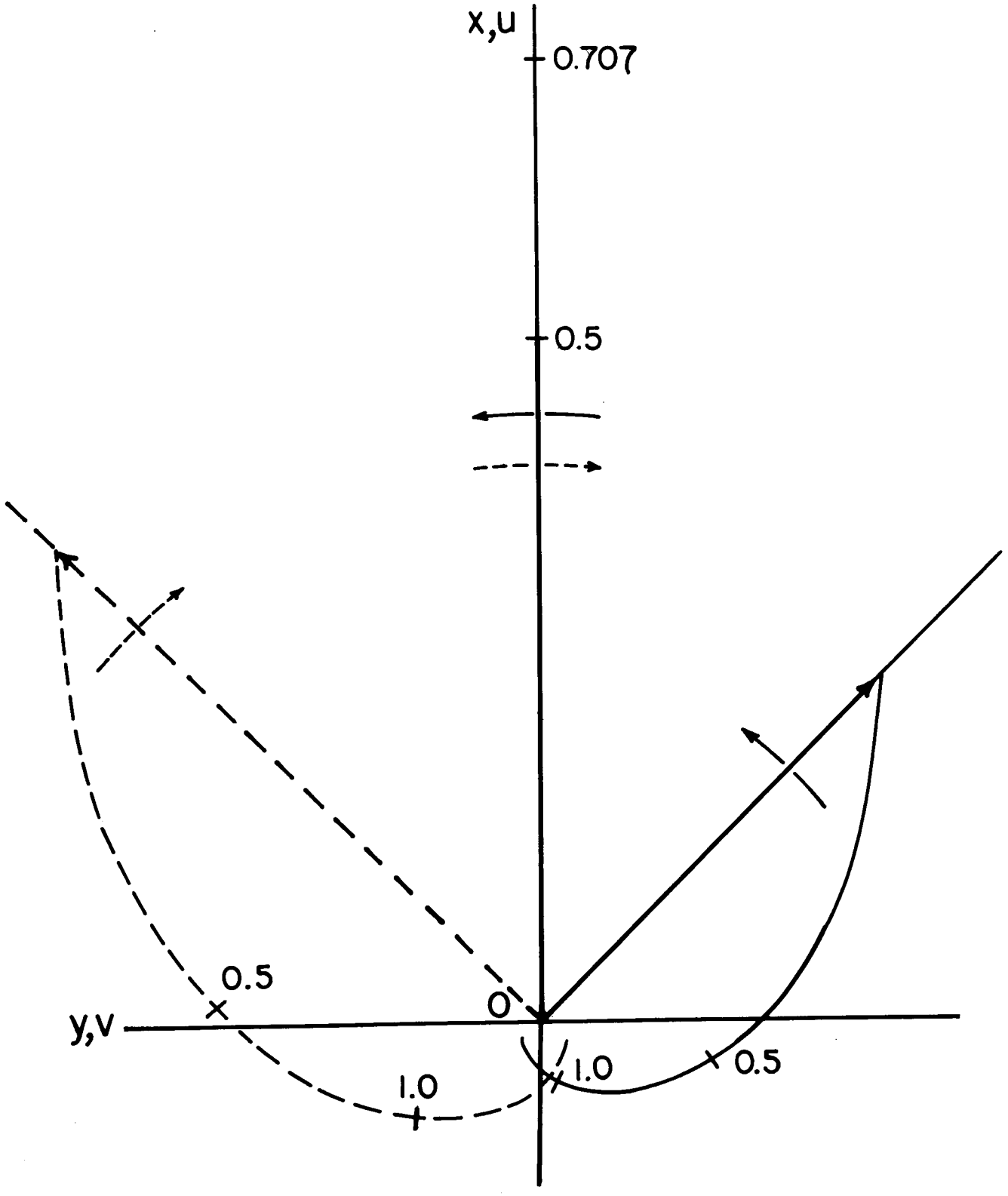
x,u
0.707
0.5
0.5
y,v
0
1.0
1.0
0.5

Figure 3. The terminal point of the surface velocity as a function of time (radians) from a numerical solution for an oscillating stress with angular frequency k = 1. Initial flow conditions were a state of rest, and the applied surface shear was given by $du/dz\big|_o = -1.414 \sin kt$. The numerical solution approaches the theoretical ellipse described in the text.

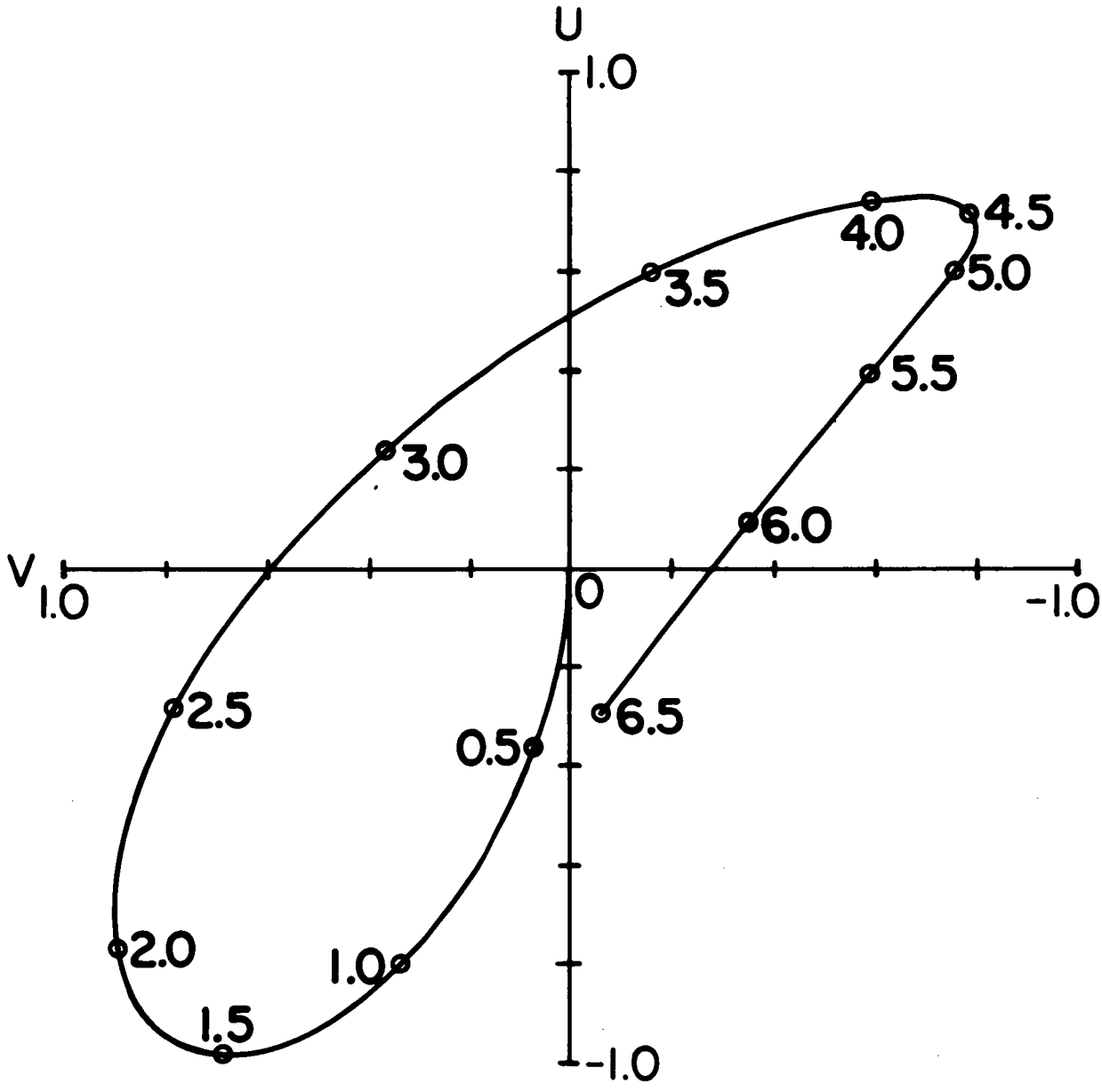
U
1.0
-1.0
V
1.0
0
-1.0
4.5
4.0
5.0
3.5
5.5
3.0
6.0
6.5
2.5
0.5
2.0
1.0
1.5

Figure 4. The terminal point of the surface velocity as a function of time (radians) from a numerical solution for an oscillating stress with angular frequency $k = 2\pi$. Initial flow conditions were a state of rest, and the applied surface shear was given by $du/dz\big|_o = 1.414 \cos kt$. The numerical solution approaches the theoretical ellipse described in the text.

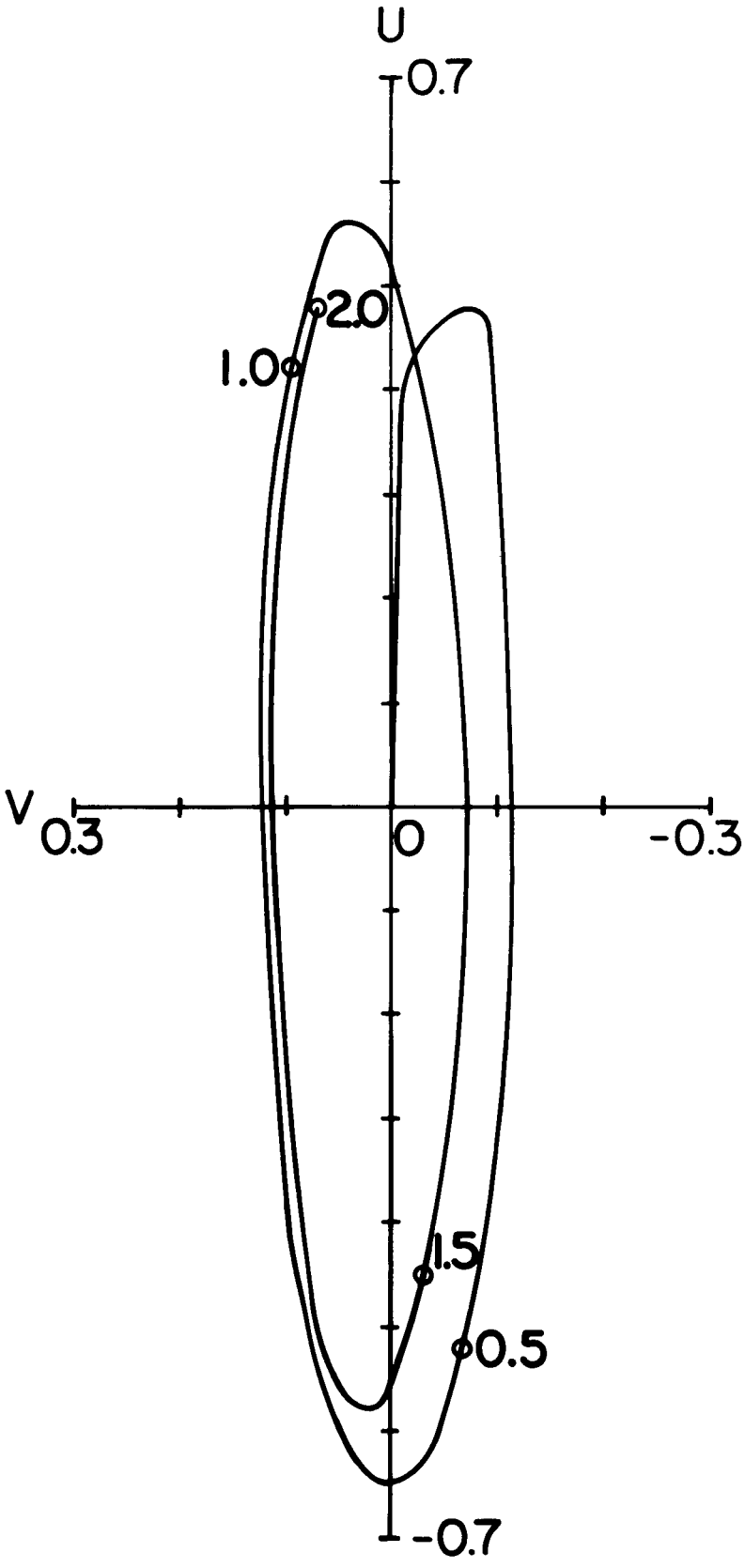
U
0.7
2.0
1.0
V
0.3
0
-0.3
1.5
0.5
-0.7

Figure 5. The terminal point of the surface velocity as a function of time (radians) from a numerical solution for an oscillating stress with angular frequency k = 2. Initial flow conditions were a state of rest, and the applied surface shear was given by $du/dz\big|_o = 1.414 \cos kt$. Resonance of the anticyclonic component ($\ell=-2$) is shown by the steady amplification of the velocity.

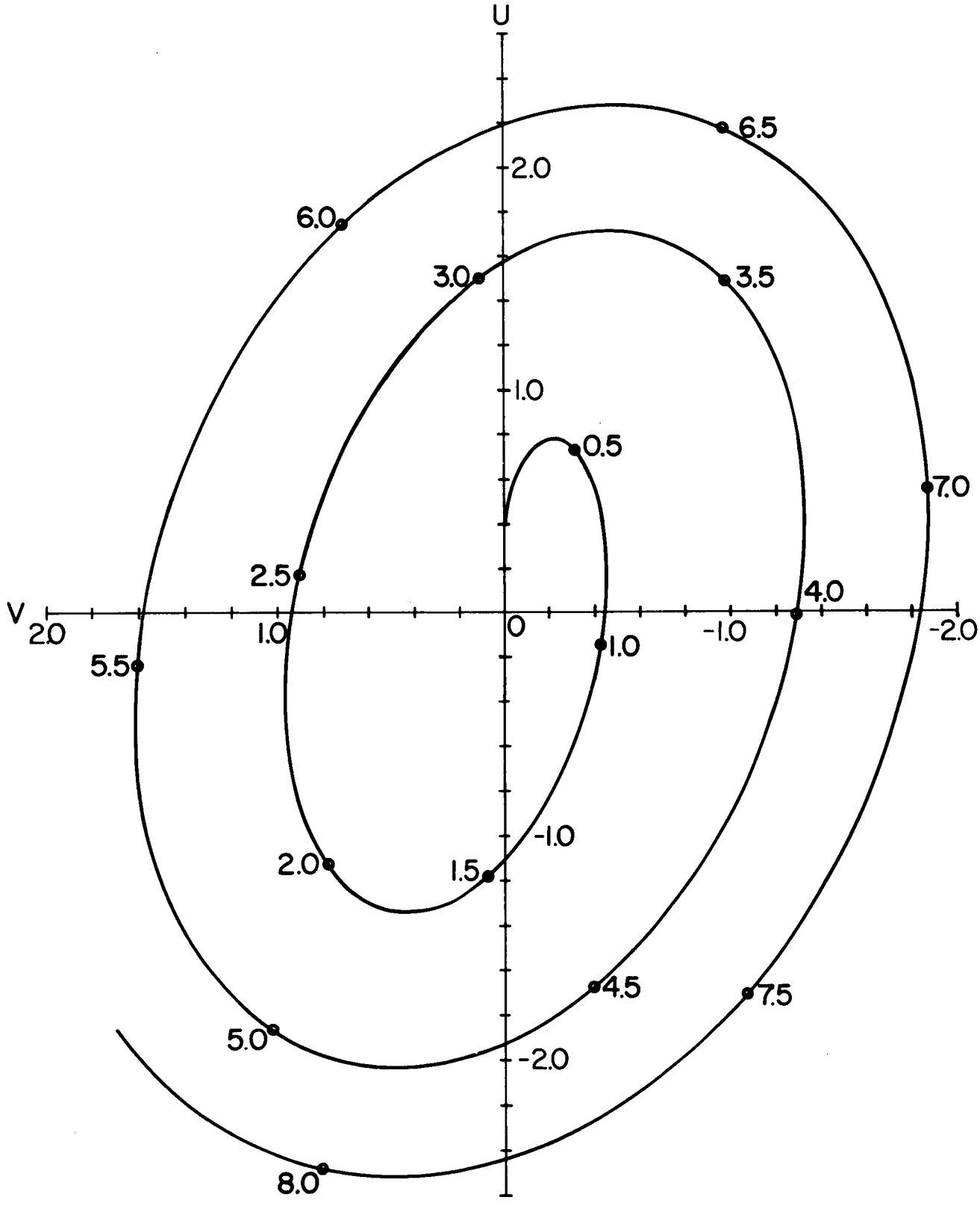
U
V
2.0
1.0
0
-1.0
-2.0
0.5
1.0
1.5
2.0
2.5
3.0
3.5
4.0
4.5
5.0
5.5
6.0
6.5
7.0
7.5
8.0

Figure 6. The terminal point of the surface velocity as a function of time (pendulum hours) for a step function in stress, from a numerical solution with constant viscosity. This result is identical with Fredholm's solution (Ekman, 1905, Figure 3).

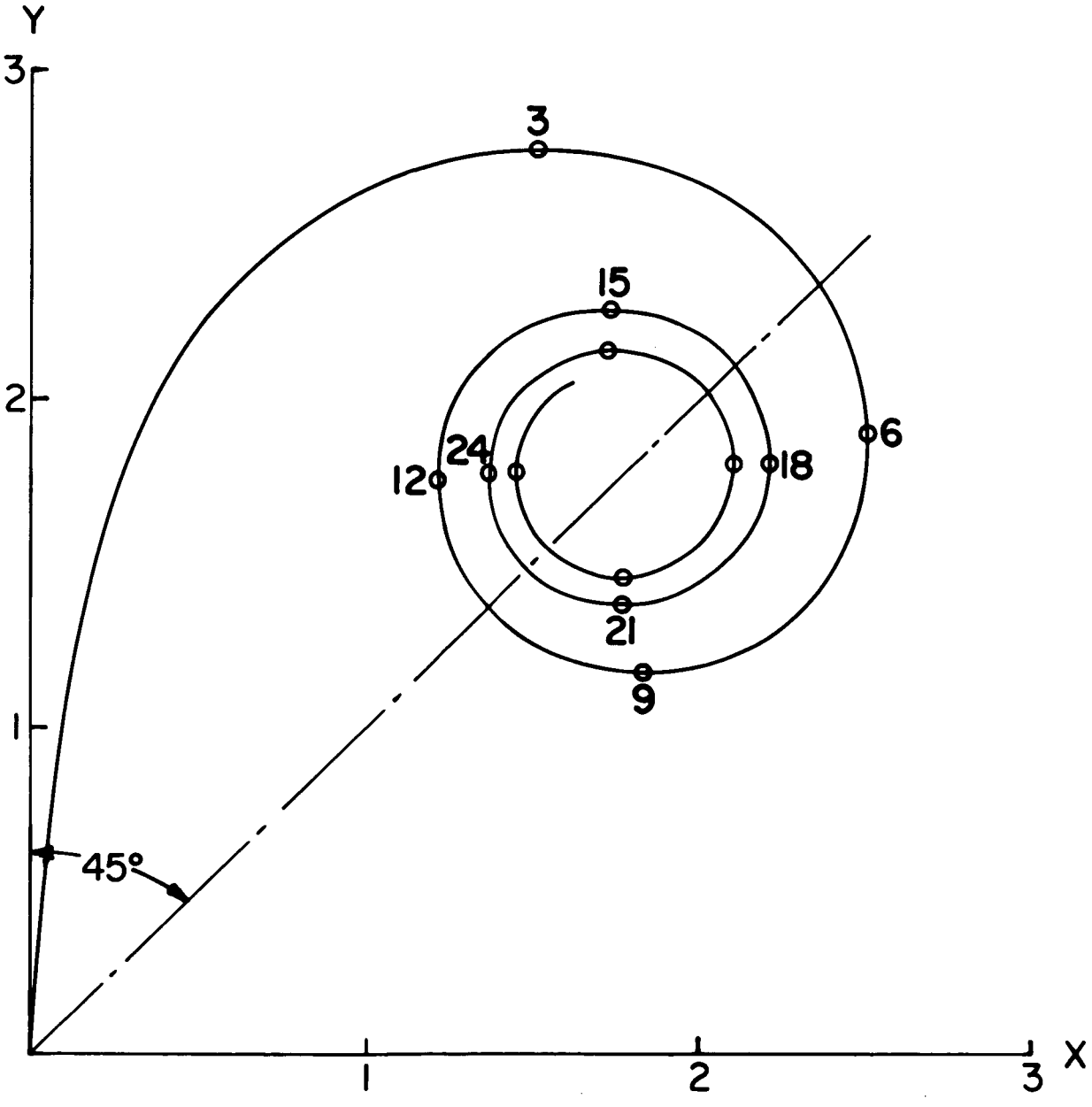
Y
3
2
1
3
15
6
24
12
18
21
9
45°
1
2
3
X

Figure 7. Terminal points of the velocity as a function of time (pendulum hours) at the depths D'= 0 (upper figure), D' = 0.5 (lower left), and D' = 1.0 (lower right), from a numerical solution for a step function in stress and with Ekman's "quadratic friction-relationship". The inertial oscillations may be seen to decay much more slowly than for the case of a constant coefficient of viscosity (Figure 6).

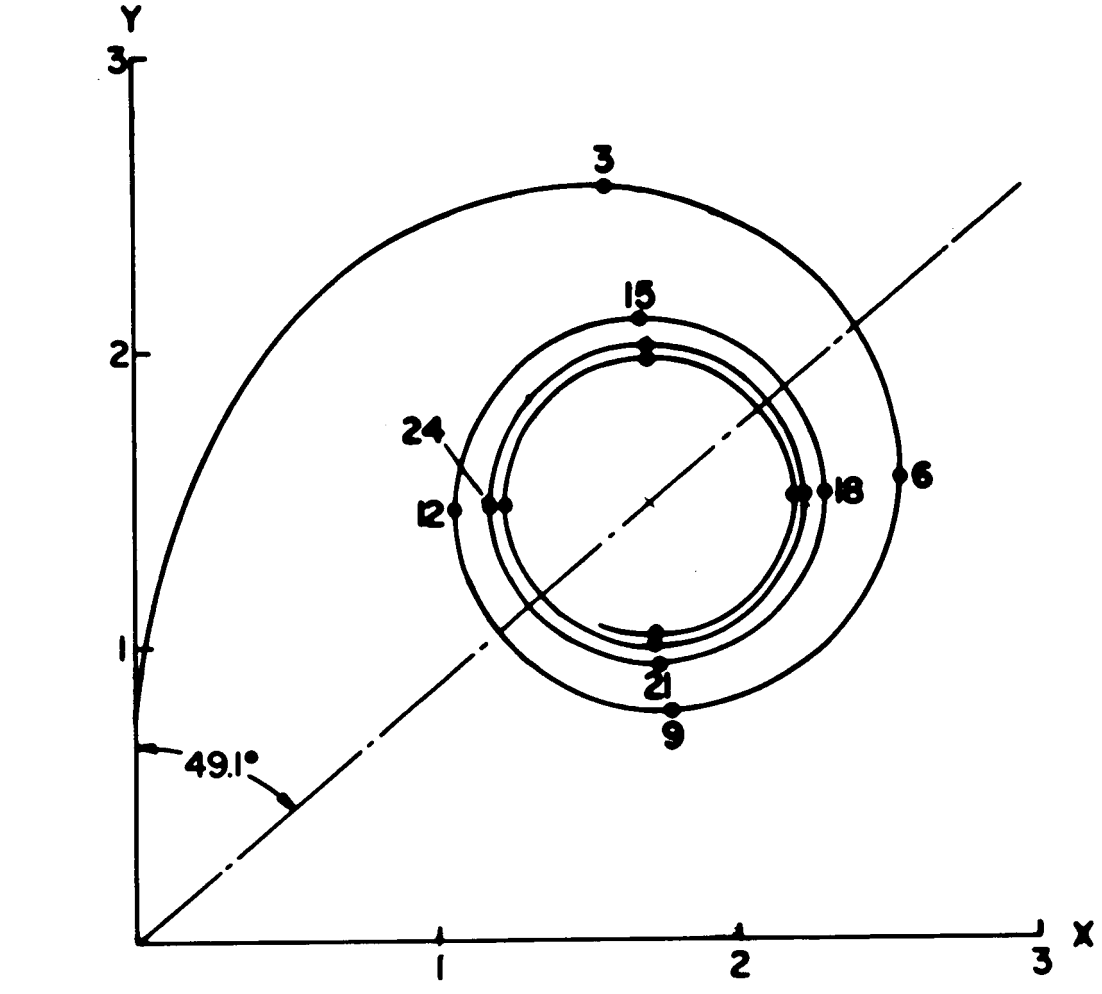
Y
3
2
1
3
15
24
12
18
6
21
9
49.1°
1
2
3
X

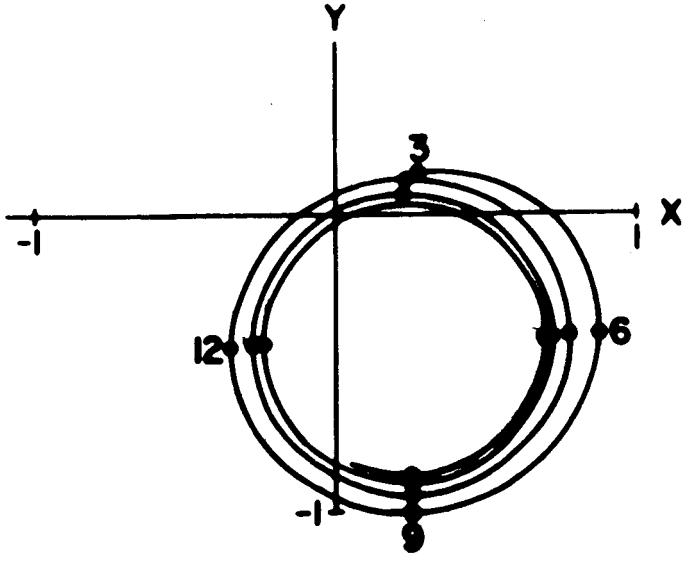
Y
3
-1
1
X
12
6
-1
9

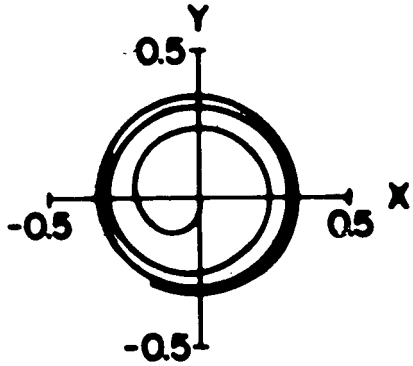
Y
0.5
-0.5
0.5
X
-0.5

Figure 8. Transitory solutions for a continuously varying wind (dashed arrows) as a function of time (radians) for the case of constant viscosity. Depths on the spiral hodagraphs are in terms of the characteristic depth D.

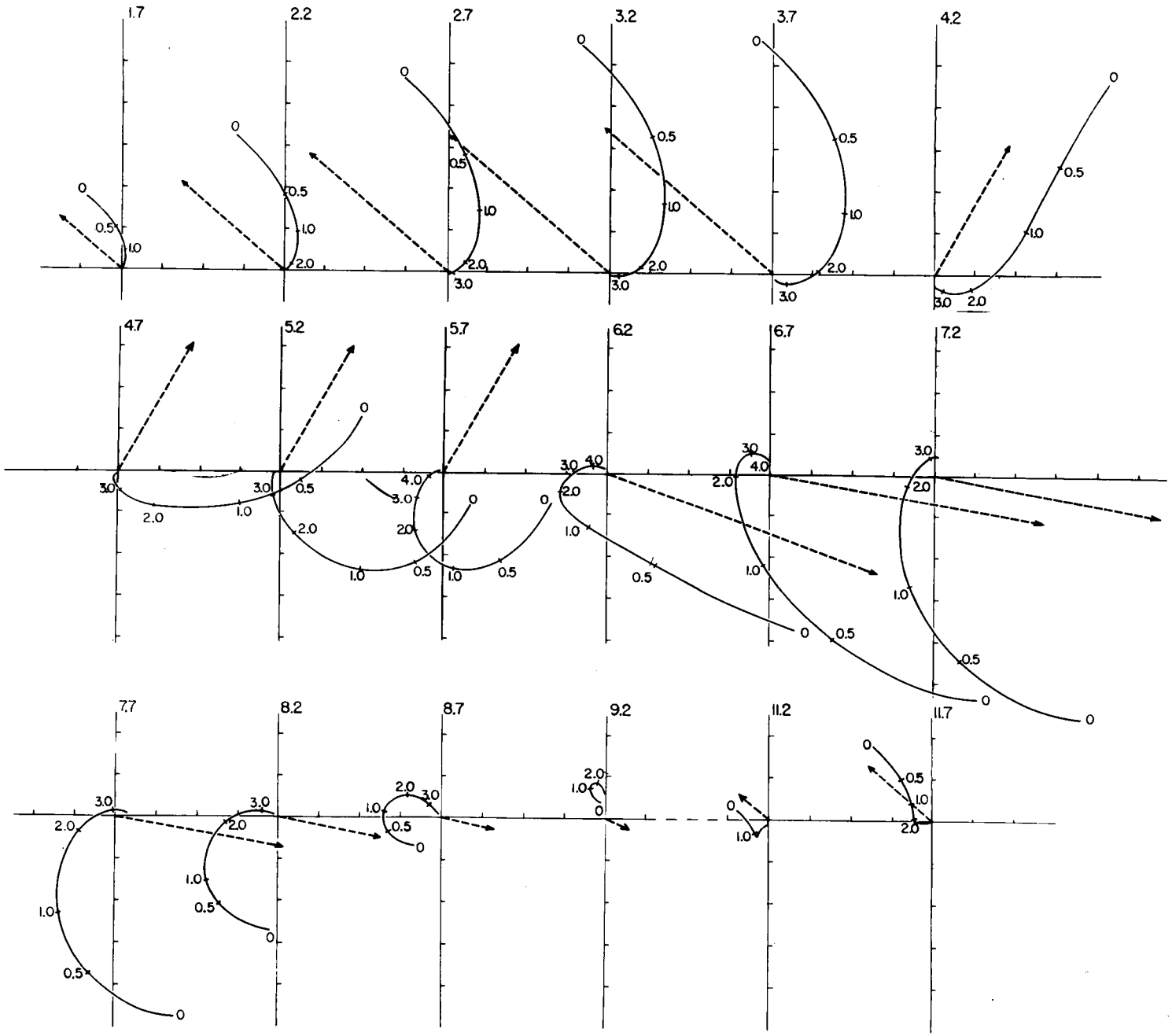
1.7
2.2
2.7
3.2
3.7
4.2
4.7
5.2
5.7
6.2
6.7
7.2
7.7
8.2
8.7
9.2
11.2
11.7

Figure 9. Transitory solutions for a continuously varying wind (dashed arrows) as a function of time (radians) for the case of the quadratic coefficient of viscosity. Flow speeds indicated by the spiral hodagraphs are in centimeters per second, wind speeds are in meters per second, and depths are in meters. The circled point on each hodagraph indicates the point of attachment of the shallow logarithmic layer.

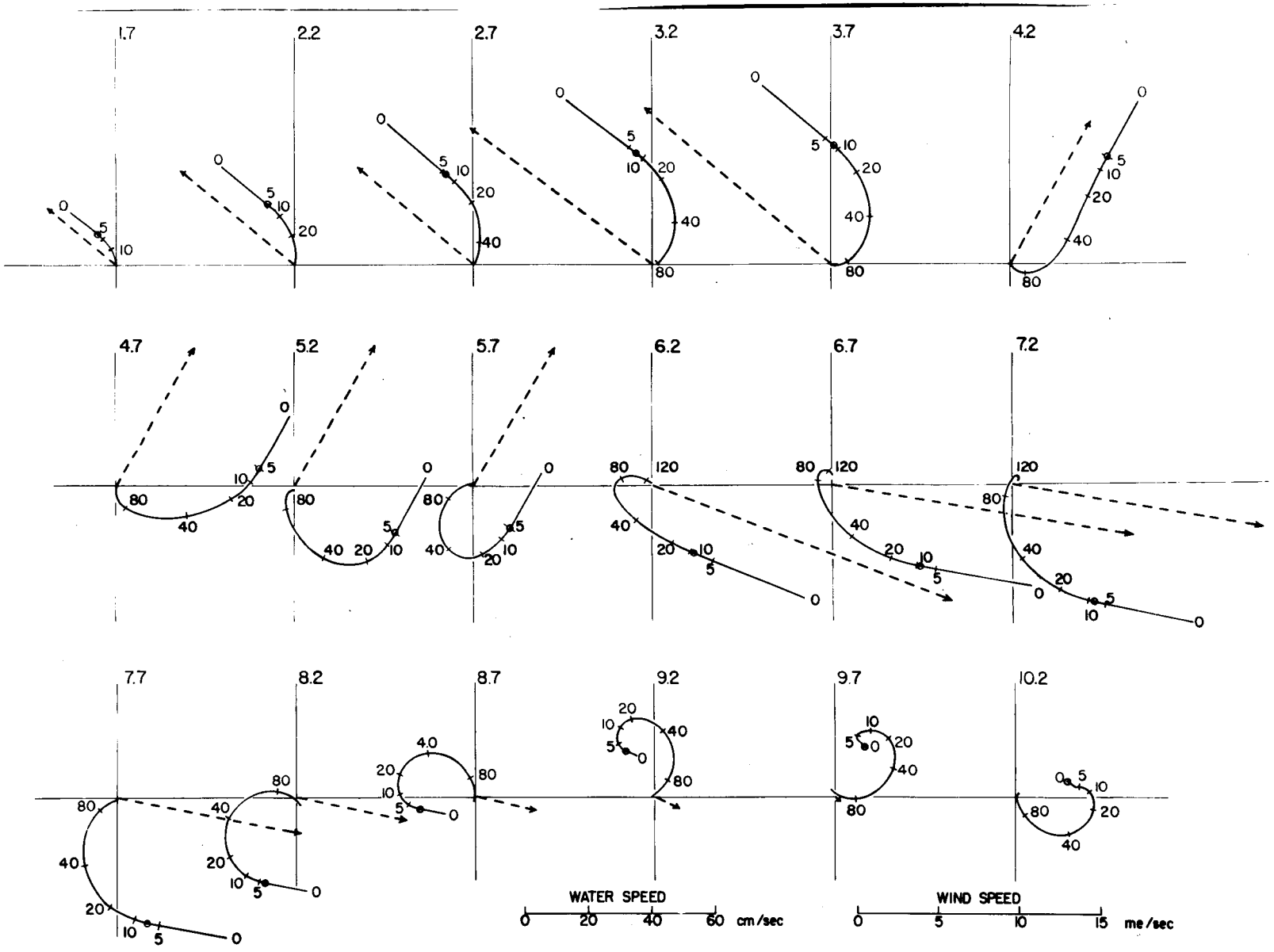
1.7
2.2
2.7
3.2
3.7
4.2
4.7
5.2
5.7
6.2
6.7
7.2
7.7
8.2
8.7
9.2
9.7
10.2
WATER SPEED
0 20 40 60 cm/sec
WIND SPEED
0 5 10 15 m/sec